Modulating Activity and Selectivity of CO_2 Electroreductions at Au-Water Interfaces via Engineering Local Cation Condition

Xueping Qin*, Tejs Vegge, Heine Anton Hansen*

Department of Energy Conversion and Storage, Technical University of Denmark, 2800 Kgs. Lyngby, Denmark.

Abstract

The mechanistic understanding of CO_2 reduction reaction (CO_2RR) under electrochemical conditions is crucial for optimizing the overall catalytic performance. While electrolyte ions have received considerable attention, it remains unclear how the condition of interfacial cations modulate the CO_2RR and the competitive hydrogen evolution reaction (HER) at electrode-electrolyte interfaces. Herein, we explore CO_2 activation and Volmer step representing the critical first electron transfer during CO_2RR and HER, respectively. This investigation involves manipulating the cation identity (K^+, Li^+, and H^+) and concentration at Au-water interfaces, which is carried out via the slow-growth sampling approach integrated with *ab initio* molecular dynamics simulations. Our results demonstrate that the high local alkali metal cation (AM^+) concentration facilitates CO_2RR following the order of $2K^+ > 1K^+ > 2Li^+ > 1Li^+ > 0AM^+$, and the highly promoted CO_2 activation kinetics originate from the short-range coordination between alkali metal cations and reaction intermediates. However, the interfacial HER behaves very differently with the kinetics order of $1Li^+ > 0AM^+ > 1K^+ > 2Li^+ > 2K^+$, closely related to the interfacial water structures, which are affected by both cation identity and local concentrations. Overall, the activity and selectivity of CO_2RR at the Au-water interface can be enhanced by increasing the local cation concentration ($K^+ > Li^+$). These findings highlight the critical roles of alkali metal cations and reaction microenvironments in modulating interfacial reaction kinetics.

Keywords: electrode-electrolyte interface, *ab initio* molecular dynamics, cation, CO_2 electroreduction, hydrogen evolution reaction

Introduction

The energy crisis has received lots of attention recently, and it has become a long-term goal to develop a sustainable society with clean energy.[1-3] Among various electrochemical technologies, electrocatalytic CO_2 reduction reaction (CO_2RR) is very attractive to convert the greenhouse gas CO_2 into useful fuels and chemicals using copper, gold, and silver as metal catalysts,[4-8] where gold catalyzes CO_2RR producing CO gas as the critical component of syngas.[6, 9] While previous studies have focused on the electrode material modification,[10-11] the crucial role of electrolyte components is non-negligible affecting interfacial electrochemical reactions, especially the recently recognized cation effect, which enhances CO_2RR via induced electric field-dipole interaction or direct coordination.[12-18] Therefore, gaining mechanistic insights into alkali metal cation effects on CO_2RR is significant.

Cations have been illustrated to affect both CO_2RR and competitive HER at electrode-electrolyte interfaces.[14-17, 19-20] For example, Koper et al. found that no CO can be produced in electrolytes without any alkali metal cations, and the cation role is ascribed to a promotion effect via coordination interaction between cations and reaction intermediates.[15] Besides, HER is found to be promoted or inhibited by tuning the local cation concentration.[20-21] As discussed by Koper et al.,[20] increasing cation concentrations at moderately alkaline pH (pH = 11), can significantly enhance the HER activity on Au electrodes. However, excessively high near-surface cation concentrations at high pH (pH = 14) reduce the HER activity due to the surface blockage effect.[20] A more recent study by Hu et al. suggests the local electric field modulated by cation accumulations at the outer Helmholtz plane (OHP) is the key to inhibiting HER via suppressing the proton diffusion, and the electric field-dipole interaction can enhance CO_2RR.[16] Theoretical simulations also illustrate that the cation effect on CO_2RR originates from the induced local electric field or short-range coordination.[13, 18, 22-24] So far, how cation modulates CO_2RR and promotes reaction kinetics is still under debate. Moreover, experiments have been carried out exploring the cation role in the HER,[20-21, 25-26] and corresponding theoretical studies are desired to better evaluate the CO_2RR selectivity. Hence, regarding the essential role of the cation on the overall CO_2RR performance, two significant issues need to be addressed as follows:

(1) How do local cations with different identities and concentrations at electrode-electrolyte interfaces affect CO_2RR and concomitant HER, respectively?

(2) What is the optimal local cation condition and reaction microenvironment to maximize the activity and selectivity of CO_2RR? What is the underlying design principle?

To study the cation effect on interfacial CO_2RR kinetics, our previous work focused on the K^+ role by constructing the Au-water interfaces, including explicit water solvents and cations.[22, 27-28] To thoroughly understand the cation modulation effect, it is necessary to consider different cation identities and various local concentrations for interfacial CO_2RR and HER. Here, three types of cations, including K^+, Li^+, and H^+, are included in the solid-liquid interfacial models, and the atomic-scale simulations focus on the first electron transfer steps involving the CO_2 activation and water dissociation during CO_2RR and HER, respectively, being the rate-determining step and initiating overall electrocatalytic interfacial reactions.[27, 29] Our results demonstrate that increasing the local alkali metal cation concentration facilitates CO_2 activation and inhibits water dissociation ($K^+ > Li^+$), thus improving both activity and selectivity of CO_2RR at Au-water interfaces.

Methods

Computational details and model setup Atomic-scale simulations are carried out based on density functional theory (DFT) via Vienna *Ab-initio* Simulations Package (VASP)[30-31] with the projector augmented wave (PAW)[32-33] method. The electron exchange-correlation interactions are described within the generalized gradient approximation (GGA) framework by the Perdew-Burke-Ernzerhof (PBE) functional.[34] The cut-off energy is set to be 400 eV. The (2 × 3) Au(110) supercell is constructed containing seven atomic layers, and the bottom four layers are fixed at bulk positions of the Au lattice, while the rest are allowed to move freely. The simulation cell size of the Au-water interfacial models is 8.32 × 8.82 × 40 $Å^3$, where a 12 Å-vacuum region in the *z* direction is left alongside the Au substrate and multiple explicit water layers, prohibiting spurious periodic interactions between interfaces. The liquid water phase

contains 44 explicit water molecules with a density of 1 g cm^{-3}. The same number of cations (including K^+, Li^+, and/or H^+ as the point charge) is introduced into simulation models to ensure similar charged states and work functions of the Au electrode. In total, two cations are added to Au-water interfacial models, and two electrons negatively charge the Au electrode to maintain overall charge neutrality, thus constructing five sets of models including 2K, 1K1H, 2Li, 1Li1H, and 2H, respectively. With these model setups, various local alkali metal cation concentrations can be reached with $2K^+$ (2K), $1K^+$ (1K1H), $2Li^+$ (2Li), $1Li^+$ (1Li1H), and $0AM^+$ (2H) at Au-water interfaces, respectively. Bader charge analysis is used to obtain the charge distributions of various components.[35-36] Due to the importance of van der Waals (vdW) forces to liquid water solvents, the zero-damping DFT-D3 method of Grimme[37] is used.

Molecular dynamics and enhanced sampling For Au-water interfacial models, *ab initio* molecular dynamics (AIMD) simulations are carried out within the canonical (NVT) ensemble at 298 K using the Nose-Hoover thermostat.[38-39] A 1.2 fs time step is used in the molecular dynamics simulations with the hydrogen mass set to 2 atomic mass units.[40] Before sampling the reaction kinetics, standard AIMD simulations are carried out to allow the solid-liquid interface and explicit solvent phase to reach the relative equilibrium state. At least three configurations are used for the subsequent constrained *ab initio* molecular dynamics (cAIMD) simulations to evaluate the activation and reaction energies, where the statistical error is also obtained. The *k*-point mesh grid of (3 × 3 × 1) is used in both standard and constrained molecular dynamics simulations. During cAIMD, the slow-growth (SG) sampling approach[41-42] is employed to evaluate the gradual evolutions from the initial state to the final state along the reaction coordinate, which is represented by defining a suitable collective variable (CV) (denoted as SG-AIMD). The transformation velocity in the sampling approach is set to be 0.001 Å/step. Such a slow-growth approach is based on thermodynamic integration, and specifically, the blue-moon ensemble, as implemented in VASP, is adopted to compute the corresponding mean force that acts on the CV along the reaction coordinate.[43] The reaction barriers and energies are obtained by collecting and integrating the free-energy gradients to plot the free energy profiles.[43-44]

Results and discussion

Using Au-water as model interfaces, K, Li, and/or H atoms are introduced into interfacial water layers, which ionize into cations (K^+, Li^+, and H^+) by transferring electrons to the Au surfaces. This electron transfer changes the interfacial dipole and the surface work function (WF), related to the applied potential, as discussed in previous work.[22, 45-46] As shown in **Figure 1** (left), two cations are presented at solid-liquid interfaces, including Au-water-2K (2K), Au-water-1K (1K1H), and Au-water-0AM (2H), where Au-water-2Li (2Li) and Au-water-1Li (1Li1H) are shown in Figure S1. With these model setups, various local AM cation concentrations are reached, where $2K^+$ ($2Li^+$), $1K^+$ ($1Li^+$), and $0AM^+$ represent the high, medium, and low interface concentrations of 0.027, 0.014, and 0 atom/$Å^2$, respectively. Correspondingly, the induced interfacial charge density distributions are similar (**Figure 1**, right). Bader charge analysis (Table S1) indicates that the Au electrode shows almost identical negatively charged states (-1.27, -1.26, and -1.19 e for $2K^+$, $1K^+$, and $0AM^+$, respectively). For interfacial structures, a 30 ps AIMD simulation was performed in Au-water-2K as described in our previous study,[22] and other solid-liquid interface models are derived from the 2K case to accelerate the Au-water-cation interface equilibration.

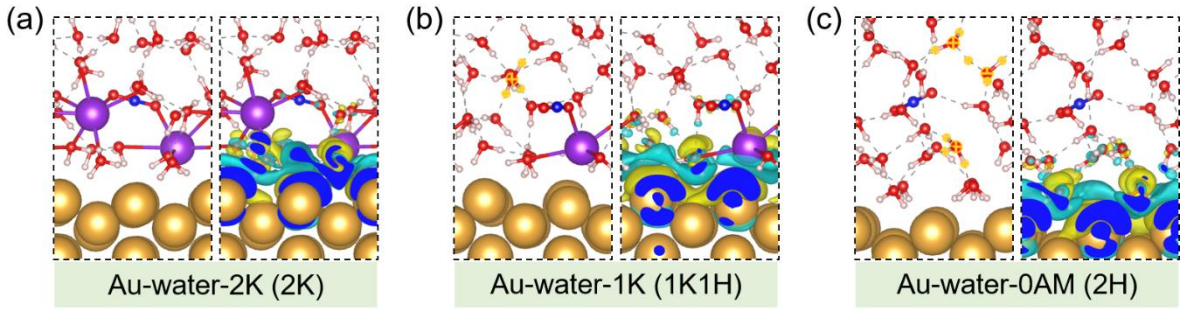

Figure 1. Simulation models (left) and interfacial charge density distributions (right) for alkali metal cation numbers of 2K (a), 1K (b), and 0AM (c). For charge distributions, yellow represents the electron accumulation, while cyan shows the electron depletion (isosurface level = 0.0008 e/bohr^3). Protons (hydronium) are shown in yellow balls. Color code: Au, golden; K, purple; C, blue; O, red; and H, white.

Under various conditions, the CO_2 activation with the first electron transfer is studied to comprehend the impact of local cation conditions on CO_2RR at electrode-electrolyte interfaces. At the Au-water interface, the collective variable (CV) is defined as the C-Au distance varying along the CO_2 adsorption onto electrode surfaces. In **Figures 2a**, **b**, and **c**, key structures, including the initial state (Initial), transition state (TS), and final state (Final) of CO_2 activation during SG-AIMD simulations are shown for 2K, 1K, and 0K, respectively. The free energy profile (**Figure 2d**) illustrates that the high alkali metal cation concentration (2K) contributes to facile reaction kinetics with the smallest energy barrier of 0.61 eV,[22, 27] and the lower cation concentration (1K) shows a higher but still surmountable barrier of 0.88 eV. However, CO_2 activation needs to overcome a much higher kinetic barrier of 1.48 eV when no alkali metal cations are present in the electrolyte (**Figure 2d**, 0AM). Regarding K cations, our simulation results show the barrier trend of 0.61 eV (2K) < 0.88 eV (1K) < 1.48 eV (0K) during CO_2 activations, explaining the previous experimental observation where CO_2 reduction rate can be accelerated by local high K cation concentrations.[47] With the alkali metal cation accumulation at the interface, CO_2RR is promoted as observed by Hu et al.,[16] which could approximately correspond to the 2K case with a small barrier of 0.61 eV. It is important to highlight the WF sampling results, revealing almost consistent potential conditions at Au-water interfaces across different alkaline metal scenarios (Table S2). Our previous work utilizing the capacitor model[48] demonstrated negligible energy correction effects on reaction kinetics and thermodynamics under constant potentials,[27] thus it is anticipated that the observed activity trend will remain unchanged.

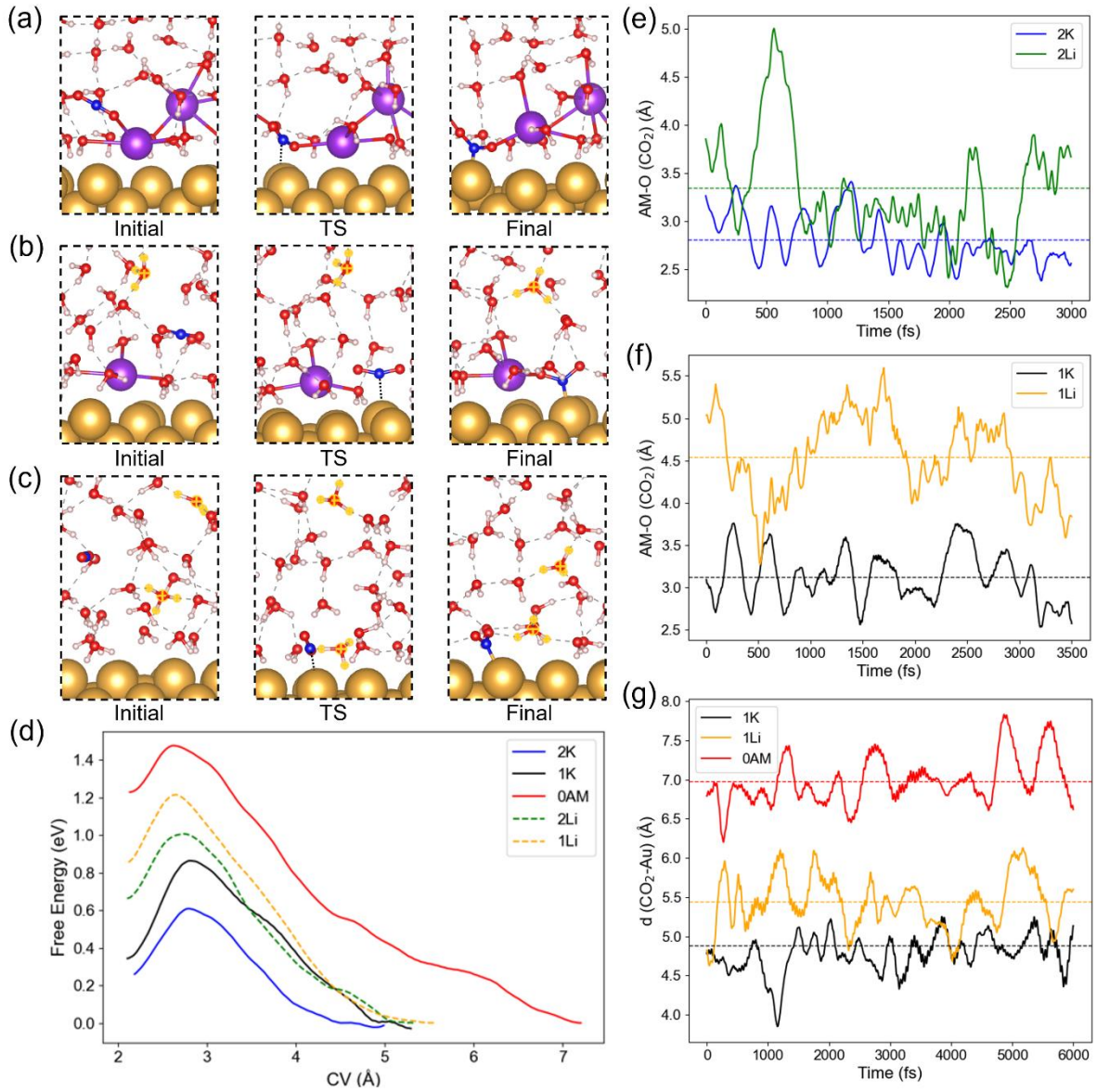

Figure 2. Key structures of CO_2 activation during SG-AIMD with 2K (a), 1K (b), and 0K (c). The corresponding free energy profile of CO_2 activation (d). The AM-O distance along CO_2 adsorption in 2K and 2Li (e) and 1K and 1Li (f) with the averaged values shown by the dashed lines. The distance between CO_2 and the Au surface during AIMD in 1K, 1Li and 0AM (g). Protons (hydronium) in b and c are shown by yellow balls.

For Li cations at Au-water interfaces, the promotion effect on CO_2 activations is weaker than for K cations. For 2Li, the CO_2 activation shows a kinetic barrier of 1.01 eV with a reaction energy of 0.67 eV, as indicated by the dashed green line in **Figure 2d**. The key structures, including the initial, transition, and final states, are shown in Figure S2a. By decreasing the local Li concentration to 1Li (Figure S2b), the free energy barrier during CO_2 activation increases to 1.21 eV with the corresponding reaction energy of 0.86 eV (**Figure 2d**, dashed orange line). As depicted in **Figure 2d**, the enhanced energy sampling results demonstrate that both the local alkali metal cation concentration and cation identity at Au-water interfaces can substantially affect the reaction kinetics of CO_2 activation, showing the activity trend of $2K^+ > 1K^+ > 2Li^+ > 1Li^+ > 0AM^+$. When analyzing the reaction kinetics and thermodynamics involved

in CO_2 activation from the bulk water phase to electrode surfaces, it is important to note that the local minimum states, including the initial, transition, and final states, are identified based on averaged forces reaching zero. It should be noted that the starting points of the sampling simulations in Au-water (0AM) and Au-water-cations (2K, 2Li, 1K, and 1Li) differ (**Figure 2d**), with the former commencing at 7.20 Å and the latter starting at around 5 to 5.5 Å. This dissimilarity is intricately linked to the interfacial interactions among CO_2 molecules, cations, water, and Au surfaces, which will be addressed subsequently.

Given the simulation results discussed above, it is essential to examine the interactions between CO_2 and cations, as well as between CO_2 and Au surfaces, within explicit solvent conditions at the electrode-electrolyte interfacial region. For the high alkali cation concentration condition (Au-water-2AM), the K-O (CO_2) and Li-O (CO_2) distances during SG-AIMD samplings in 2K and 2Li systems are analyzed, respectively. **Figure 2e** illustrates that 2K cations show stronger interactions with the CO_2 molecule via short-range coordination with the shorter averaged AM-O distance (2.81 Å, dashed blue line) compared to 2Li (3.35 Å, dashed green line). It can also be observed that Li cations don't coordinate with the $*CO_2$ at the end of adsorption on Au surfaces with Li-O distances of 3.61 and 3.79 Å, and $*CO_2$ is stabilized by four hydrogen bonds (Figure S3a). Contrastingly, 2K cations maintain coordination with $*CO_2$, featuring K-O distances of 2.57 and 2.61 Å. Additionally, one extra hydrogen bond contributes to the stabilization of $*CO_2$ at the interface (Figure S3b). When the metal cation concentration (Au-water-1AM) is lowered, similar phenomena are observed, where 1K shows stronger interaction with the key $*CO_2$ intermediate than 1Li (**Figure 2f**). Considering the final state of $*CO_2$ at Au-water-1AM interfaces, 1Li shows no binding to the $*CO_2$ with the Li-O distance of 3.98 Å (Figure S3c), and 1K binds closely to $*CO_2$ with the K-O bond of 2.82 Å (Figure S3d). There are no AM-O interactions for non-metal-cation interfaces (Au-water-0AM), and three hydrogen bonds stabilize the $*CO_2$. The AM-O distances between cations and $*CO_2$, as well as the hydrogen bonds between water and $*CO_2$, are summarized in **Table 1**, which further highlights the importance of stabilization effects induced by alkali metal cations at Au-water interfaces (K-O > Li-O > H-O), thereby affecting the thermodynamics and kinetics of CO_2 activation reaction ($2K^+ > 1K^+ > 2Li^+ > 1Li^+ > 0AM^+$).

Table 1. The AM-O ($*CO_2$) distances (Å), AM-O ($*CO_2$) bond number, H-O ($*CO_2$) distance (Å), and hydrogen bond number are summarized for Au-water-2AM, Au-water-1AM, and Au-water-0AM systems.

Systems	AM-O ($*CO_2$) distance	AM-O ($*CO_2$) bond number	H-O ($*CO_2$) distance	Hydrogen bond number ($*CO_2$)
2Li[#]	3.61 & 3.79	0	1.46 &1.78 & 1.87 & 1.91	4
2K	2.57 & 2.61	2	1.86	1
1Li[#]	3.98	0	1.60 & 1.61 & 1.99 & 2.08	4
1K	2.82	1	1.44 & 1.71 & 1.95	3
0AM	/	/	1.72 & 1.72 & 1.92	3

[#]It should be noted that, even though there is no AM-O bond in the $*CO_2$ final state on Au surfaces for 2Li and 1Li, the coordination interaction between Li cations and CO_2 exists along SG-AIMD simulations, facilitating the CO_2 activation as compared to 0AM.

The distinction between cation-deficient and cation-containing systems becomes evident when examining the initial position in CO_2 adsorption sampling simulations, which starts from 7.2 Å at the Au-water-0AM interface, as depicted in **Figure 2d**. The CO_2-Au distance is monitored

during a standard AIMD simulation. As depicted in **Figure 2g** (red line), the Au-water-0AM system demonstrates fluctuations in the distance between CO_2 and the Au surface, maintaining a relatively steady value of approximately 7 Å. Such a large distance keeps the inert CO_2 molecule far from electrodes, resulting in a high kinetic barrier (1.48 eV) for activation. The distance variations at Au-water-1AM are inserted for comparison, with the averaged CO_2-Au distance of 4.88 and 5.44 Å for 1K (black, **Figure 2g**) and 1Li (orange, **Figure 2g**), respectively. The contrast between Au-water-0AM and Au-water-1AM reveals that the CO_2 molecule is drawn closer to the electrode surface in cation-containing electrolytes. Conversely, there is no driving force for CO_2 to approach Au electrodes in cation-deficient electrolytes. Overall, the CO_2 activation at Au-water interfaces is significantly influenced by both cation identity and concentration, and interactions among CO_2, cations, water, and Au electrodes collectively impact interfacial reaction thermodynamics and kinetics.

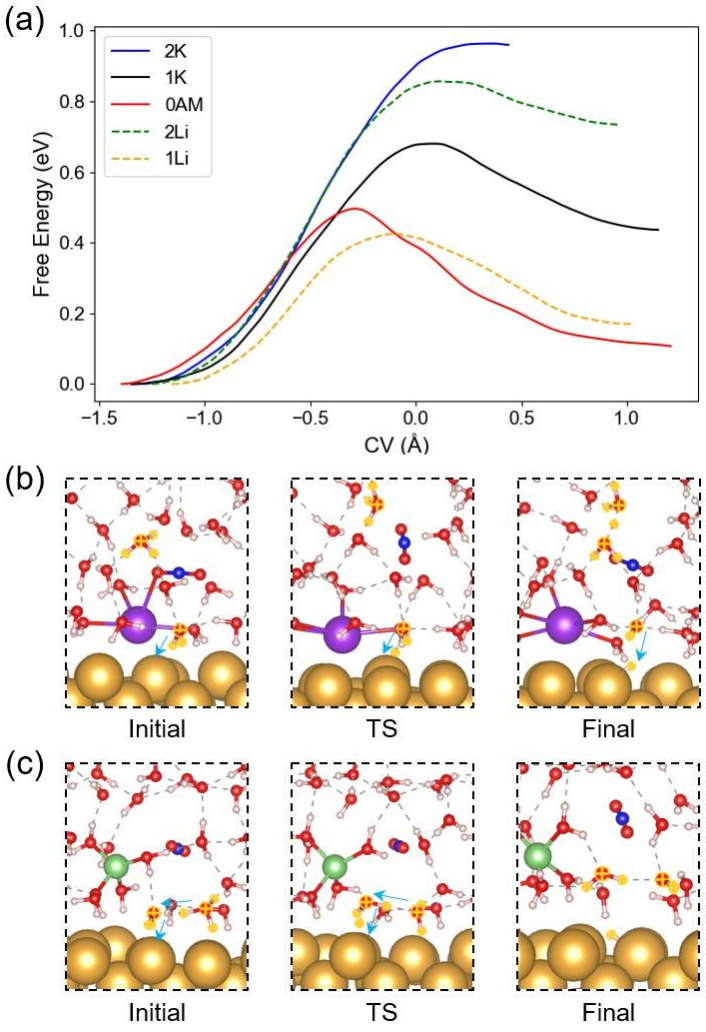

Figure 3. The free energy profile of the Volmer step (a). Key structures of the Volmer step in the HER during SG-AIMD in 1K (b) and 1Li (c). Protons (hydronium) are shown by yellow balls, and light blue arrows indicate proton transfer.

In the meantime, it is worthwhile to explore the HER kinetics under different interfacial conditions, which are concomitant and competitive to the CO_2RR at Au-water interfaces, and the first electron transfer step involved in the Volmer reaction is considered. Unlike the CO_2 activation with a defined simple CV (C-Au distance), proton transfer occurs in HER involving

water solvents, hydronium, and Au surfaces, and the CV is defined as the combination of O-H bond cleavage and H-Au bond formation (Figure S4). It should be mentioned that various other CVs, including the simple O-H bond cleavage and additional proton shuttling among hydronium and water solvents, are also tested, showing a negligible effect on the kinetics evaluation (Figure S5). At high cation concentration at the interface, water as the proton source dissociates, producing adsorbed hydrogen (*H) with the hydroxyl species bonded to the cations in the final states (Figure S6a, 2K and Figure S6b, 2Li). This high alkali metal cation concentration prohibits the Volmer step with a quite high energy barrier of 0.97 eV in 2K and 0.86 eV in 2Li (**Figure 3a**), with 2Li exhibiting less suppression compared to 2K.

When lowering the cation concentration to 1K (**Figure 3b**), the free energy barrier during water dissociation is only 0.68 eV (**Figure 3a**, black), much smaller than that in 2K, demonstrating faster reaction kinetics. It should be noted that three hydrogen bonds stabilize the produced hydroxyl, and the proton exists in the form of Zundel cation ($H_5O_2^+$) in the final state (**Figure 3b**, Final). It is anticipated that the hydroxyl could diffuse away from the interface due to the local pH gradient, being neutralized by the proton from the Zundel cation.[49] Similarly, the 1Li interface (**Figure 3a,** dashed orange) shows faster Volmer kinetics than the 2Li interface (**Figure 3a,** dashed green) with a small reaction barrier of 0.42 eV, and key structures during Volmer step are shown in **Figure 3c.** Besides the difference in reaction kinetics (1Li > 1K), the cation identity also affects interfacial structures. The distinction between 1K and 1Li is evident in **Figures 3b** and **3c**, where K exhibits partial solvation with a closer proximity to the Au electrode, whereas four water molecules fully solvate Li. This aligns with a recent experiment-theory joint study on specific cation adsorption during the CO_2RR.[50] Unlike 1K, where hydronium is situated far from the Au surface (**Figure 3b**), the proton in 1Li rapidly diffuses from bulk water, approaching the electrode surface (Figure S7), which contributes to more effective neutralization of produced hydroxyl ions and thus faster reaction kinetics. The reaction barrier in 1Li is smaller than 0AM, where the interfacial hydronium serves as the proton source with a barrier of 0.50 eV (**Figure 3a**). A simulation with water as the proton source in 0AM shows a slightly higher reaction barrier of 0.68 eV, where the nearby hydronium neutralizes the produced hydroxyl, lowering the reaction energy (Figure S8). Based on above results, the Volmer reaction kinetics follows the order of $1Li^+ > 0AM^+ > 1K^+ > 2Li^+ > 2K^+$.

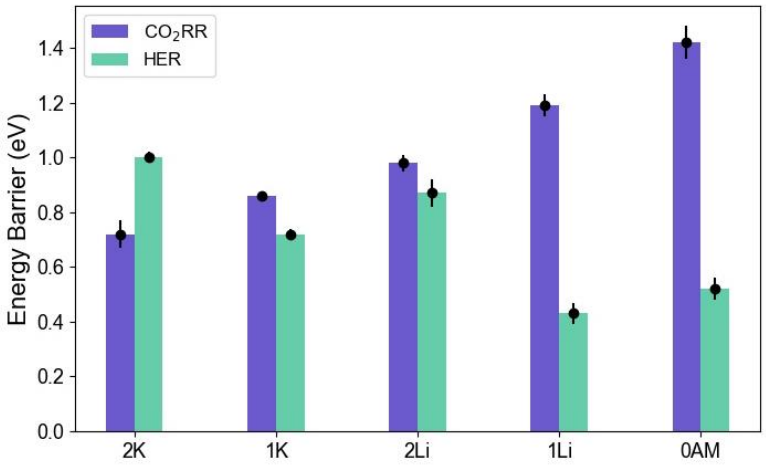

Figure 4. CO_2RR (CO_2 activation) and HER (Volmer step) energy barriers with various local cation conditions, including 2K, 1K, 2Li, 1Li, and 0AM. Error bars are obtained based on three individual sampling simulations.

Considering the microenvironment at Au-water interfaces, the kinetic free energy barriers of CO_2 activation and water dissociation under different conditions (including cation identity and concentration) are summarized in **Figure 4**, including 2K, 1K, 2Li, 1Li, and 0AM. To guarantee the data accuracy and reliability, three independent SG-AIMD simulations are performed based on different initial structures showing negligible error bars and no effect on the overall trend, and the data are summarized in Table S3. With various interfacial cation conditions, CO_2 activation including both kinetics and thermodynamics, follows the trend $2K^+ > 1K^+ > 2Li^+ > 1Li^+ > 0AM^+$ (**Figure 4**), which is mainly due to the promotion effect from AM-O (CO_2) interactions especially for K cations. Nevertheless, a distinct trend emerges during the Volmer step in HER with the order of $1Li^+ > 0AM^+ > 1K^+ > 2Li^+ > 2K^+$ (**Figure 4**), which suggests that Li exhibits superior performance compared to K,[50] especially at lower cation concentrations at interfaces.

As mentioned in one recent study,[50-51] the HER kinetics can be closely related to the hydrogen bond network and available interfacial water molecules at Pt-water interfaces. Generally, a well-connected hydrogen bond network is suggested to form a highway for delivering protons to the electrode surface, which is crucial in hydrogen electrocatalysis.[51] We further analyze the statistical distribution of hydrogen bonds along the z direction with the distance to Au surfaces (Figure S9). The hydrogen bond connectivity trend across most interfaces is found to follow the order of 0AM > 1K > 2Li > 2K (Figure S9), consistent with the HER trend illustrated in **Figure 4**. However, an exception is noted in the case of 1Li (Figure S9, dashed orange line), exhibiting the highest HER kinetics despite a disrupted hydrogen bond network. This phenomenon is likely attributed to the observed rapid proton diffusion from bulk water to electrode surfaces (Figure S7).

Overall, the local cation conditions significantly impact both CO_2RR and HER at Au-water interfaces. Higher interfacial cation concentrations prove beneficial for enhancing the CO_2RR and suppressing the competing HER, thereby influencing both activity and selectivity. Our findings reveal that optimizing CO_2RR selectivity at Au-water-cation interfaces is achieved by increasing local alkali cation concentration (2K > 1K > 0K), with an optimal surface coverage of 0.027 atom/Å^2 in 2K, effectively suppressing HER. Experimental evidence by Sargent and co-workers[47] aligns with our theoretical results, emphasizing the positive role of local alkali cations (K) in facilitating CO_2RR and inhibiting HER. It is crucial to note that the Au-water-cation interfaces exhibit a high applied potential, characterized by a significant overpotential according to the WF sampling results (Table S2). One previous experiment indicates that K displays higher HER activity compared to Li,[52] seemingly contradictory to our findings. However, this inconsistency can be attributed to the high overpotential in our simulations. Experimental data with more negative applied potentials show a reversed trend (Li > K).[52] Additionally, it is important to note that the interfacial reaction kinetics are influenced by various factors, including near-surface cation concentration, cation identity, applied potentials, and bulk/local pH.

Conclusion

In summary, we explore the impact of local cation conditions on CO_2RR using an Au-water interface model. Various cation scenarios, including 2K, 1K, 2Li, 1Li, and 0AM, are investigated to vary cation concentrations and identities. Employing *ab initio* molecular dynamics and slow-growth sampling simulations, we systematically evaluate the reaction

kinetics of CO_2 activation in CO_2RR and the Volmer step in HER. The CO_2RR kinetics follows the trend of $2K^+ > 1K^+ > 2Li^+ > 1Li^+ > 0AM^+$. Increasing the local cation concentration and replacing Li by K ions, CO_2 activation is highly facilitated via short-range interactions between cations and intermediates, while the concomitant Volmer reaction during HER is prohibited, thus improving both the activity and selectivity of CO_2RR at Au-water interfaces. The study underscores the crucial role of alkali metal cations and the local environment in electrode-electrolyte interface kinetics. Our findings not only add significant insights into the atomic-scale mechanistic understanding of CO_2RR, but also accommodate past and present experimental efforts to modulate the interfacial reactions for promoted CO_2 electrolysis (e.g., ionomer-coating,[18] cation-augmenting layers,[47] and ionic liquid electrolytes[53]). Collaborative efforts between theory/computations and experiments, coupled with precise electrochemical interface engineering, are desired to advance the design of more efficient (CO_2) electrolysis cells.

Supporting information

Supporting Information is available free of charge, including additional models, energy profiles, and statistical distribution analysis of interfacial structures.

Corresponding author

xueqi@dtu.dk

heih@dtu.dk

Declaration of interests

The authors declare no competing financial interests.

Acknowledgements

This work is supported by the Carlsberg Foundation through the Carlsberg Foundation Young Researcher Fellowship (CF19-0304). T.V. and H.A.H. acknowledge funding from the Villum Foundation through the research center V-Sustain (#9455), and the Pioneer Center for Accelerating P2X Materials Discovery, DNRF Grant number P3.

References

(1) Chu, S.; Majumdar, A., Opportunities and Challenges for a Sustainable Energy Future. *Nature* **2012,** *488*, 294-303.

(2) Sanz-Pérez, E. S.; Murdock, C. R.; Didas, S. A.; Jones, C. W., Direct Capture of CO_2 from Ambient Air. *Chem. Rev.* **2016,** *116*, 11840-11876.

(3) Seh, Z. W.; Kibsgaard, J.; Dickens, C. F.; Chorkendorff, I.; Nørskov, J. K.; Jaramillo, T. F., Combining Theory and Experiment in Electrocatalysis: Insights into Materials Design. *Science* **2017,** *355*, eaad4998.

(4) Kuhl, K. P.; Hatsukade, T.; Cave, E. R.; Abram, D. N.; Kibsgaard, J.; Jaramillo, T. F., Electrocatalytic Conversion of Carbon Dioxide to Methane and Methanol on Transition Metal Surfaces. *J. Am. Chem. Soc.* **2014,** *136*, 14107-14113.

(5) Kuhl, K. P.; Cave, E. R.; Abram, D. N.; Jaramillo, T. F., New Insights into the Electrochemical Reduction of Carbon Dioxide on Metallic Copper Surfaces. *Energy Environ. Sci.* **2012,** *5*, 7050-7059.
(6) Hori, Y.; Murata, A.; Kikuchi, K.; Suzuki, S., Electrochemical Reduction of Carbon Dioxides to Carbon Monoxide at a Gold Electrode in Aqueous Potassium Hydrogen Carbonate. *Chem. Commun.* **1987**, 728-729.
(7) Liu, S.; Tao, H.; Zeng, L.; Liu, Q.; Xu, Z.; Liu, Q.; Luo, J.-L., Shape-Dependent Electrocatalytic Reduction of CO_2 to CO on Triangular Silver Nanoplates. *J. Am. Chem. Soc.* **2017,** *139*, 2160-2163.
(8) Zhu, S.; Li, T.; Cai, W.-B.; Shao, M., CO_2 Electrochemical Reduction As Probed through Infrared Spectroscopy. *ACS Energy Lett.* **2019,** *4*, 682-689.
(9) Fu, J.; Wang, Y.; Liu, J.; Huang, K.; Chen, Y.; Li, Y.; Zhu, J.-J., Low Overpotential for Electrochemically Reducing CO_2 to CO on Nitrogen-Doped Graphene Quantum Dots-Wrapped Single-Crystalline Gold Nanoparticles. *ACS Energy Lett.* **2018,** *3*, 946-951.
(10) Hall, A. S.; Yoon, Y.; Wuttig, A.; Surendranath, Y., Mesostructure-Induced Selectivity in CO_2 Reduction Catalysis. *J. Am. Chem. Soc.* **2015,** *137*, 14834-14837.
(11) Welch, A. J.; DuChene, J. S.; Tagliabue, G.; Davoyan, A.; Cheng, W.-H.; Atwater, H. A., Nanoporous Gold as a Highly Selective and Active Carbon Dioxide Reduction Catalyst. *ACS Appl. Energy Mater.* **2019,** *2*, 164-170.
(12) Moura de Salles Pupo, M.; Kortlever, R., Electrolyte Effects on the Electrochemical Reduction of CO_2. *ChemPhysChem* **2019,** *20*, 2926-2935.
(13) Ringe, S.; Clark, E. L.; Resasco, J.; Walton, A.; Seger, B.; Bell, A. T.; Chan, K., Understanding Cation Effects in Electrochemical CO_2 Reduction. *Energy Environ. Sci.* **2019,** *12*, 3001-3014.
(14) Monteiro, M. C. O.; Dattila, F.; López, N.; Koper, M. T. M., The Role of Cation Acidity on the Competition between Hydrogen Evolution and CO_2 Reduction on Gold Electrodes. *J. Am. Chem. Soc.* **2022,** *144*, 1589-1602.
(15) Monteiro, M. C. O.; Dattila, F.; Hagedoorn, B.; García-Muelas, R.; López, N.; Koper, M. T. M., Absence of CO_2 Electroreduction on Copper, Gold and Silver Electrodes without Metal Cations in Solution. *Nat. Catal.* **2021,** *4*, 654-662.
(16) Gu, J.; Liu, S.; Ni, W.; Ren, W.; Haussener, S.; Hu, X., Modulating Electric Field Distribution by Alkali Cations for CO_2 Electroreduction in Strongly Acidic Medium. *Nat. Catal.* **2022,** *5*, 268-276.
(17) Ren, W.; Xu, A.; Chan, K.; Hu, X., A Cation Concentration Gradient Approach to Tune the Selectivity and Activity of CO2 Electroreduction. *Angew. Chem. Int. Ed. n/a*.
(18) Shin, S.-J.; Choi, H.; Ringe, S.; Won, D. H.; Oh, H.-S.; Kim, D. H.; Lee, T.; Nam, D.-H.; Kim, H.; Choi, C. H., A Unifying Mechanism for Cation Effect Modulating C1 and C2 Productions from CO_2 Electroreduction. *Nat. Commun.* **2022,** *13*, 5482.
(19) Wang, Y.; Liu, X.; Liu, J.; Al-Mamun, M.; Wee-Chung Liew, A.; Yin, H.; Wen, W.; Zhong, Y. L.; Liu, P.; Zhao, H., Electrolyte Effect on Electrocatalytic Hydrogen Evolution Performance of One-Dimensional Cobalt–Dithiolene Metal–Organic Frameworks: A Theoretical Perspective. *ACS Appl. Energy Mater.* **2018,** *1*, 1688-1694.
(20) Goyal, A.; Koper, M. T. M., The Interrelated Effect of Cations and Electrolyte pH on the Hydrogen Evolution Reaction on Gold Electrodes in Alkaline Media. *Angew. Chem. Int. Ed.* **2021,** *60*, 13452-13462.
(21) Goyal, A.; Koper, M. T. M., Understanding the role of mass transport in tuning the hydrogen evolution kinetics on gold in alkaline media. *J. Chem. Phys.* **2021,** *155*, 134705.
(22) Qin, X.; Vegge, T.; Hansen, H. A., CO_2 Activation at Au(110)–Water Interfaces: An *Ab Initio* Molecular Dynamics Study. *J. Chem. Phys.* **2021,** *155*, 134703.
(23) Chen, L. D.; Urushihara, M.; Chan, K.; Nørskov, J. K., Electric Field Effects in Electrochemical CO_2 Reduction. *ACS Catal.* **2016,** *6*, 7133-7139.
(24) Resasco, J.; Chen, L. D.; Clark, E.; Tsai, C.; Hahn, C.; Jaramillo, T. F.; Chan, K.; Bell, A. T., Promoter Effects of Alkali Metal Cations on the Electrochemical Reduction of Carbon Dioxide. *J. Am. Chem. Soc.* **2017,** *139*, 11277-11287.
(25) Liu, E.; Li, J.; Jiao, L.; Doan, H. T. T.; Liu, Z.; Zhao, Z.; Huang, Y.; Abraham, K. M.; Mukerjee, S.; Jia, Q., Unifying the Hydrogen Evolution and Oxidation Reactions Kinetics in Base by Identifying the Catalytic Roles of Hydroxyl-Water-Cation Adducts. *J. Am. Chem. Soc.* **2019,** *141*, 3232-3239.

(26) Shah, A. H.; Zhang, Z.; Huang, Z.; Wang, S.; Zhong, G.; Wan, C.; Alexandrova, A. N.; Huang, Y.; Duan, X., The Role of Alkali Metal Cations and Platinum-Surface Hydroxyl in the Alkaline Hydrogen Evolution Reaction. *Nat. Catal.* **2022,** *5*, 923-933.
(27) Qin, X.; Vegge, T.; Hansen, H. A., Cation-Coordinated Inner-Sphere CO_2 Electroreduction at Au–Water Interfaces. *J. Am. Chem. Soc.* **2023,** *145*, 1897-1905.
(28) Qin, X.; Hansen, H. A.; Honkala, K.; Melander, M. M., Cation-Induced Changes in the Inner- and Outer-Sphere Mechanisms of Electrocatalytic CO_2 Reduction. *Nat. Commun.* **2023,** *14*, 7607.
(29) Wuttig, A.; Yaguchi, M.; Motobayashi, K.; Osawa, M.; Surendranath, Y., Inhibited Proton Transfer Enhances Au-Catalyzed CO_2-to-Fuels Selectivity. *Proc. Natl. Acad. Sci.* **2016,** *113*, E4585.
(30) Kresse, G.; Hafner, J., Ab Initio Molecular Dynamics for Liquid Metals. *Phys. Rev. B* **1993,** *47*, 558-561.
(31) Kresse, G.; Furthmüller, J., Efficiency of Ab-Initio Total Energy Calculations for Metals and Semiconductors Using a Plane-Wave Basis Set. *Comput. Mater. Sci.* **1996,** *6*, 15-50.
(32) Blöchl, P. E., Projector Augmented-Wave Method. *Phys. Rev. B* **1994,** *50*, 17953-17979.
(33) Kresse, G.; Joubert, D., From Ultrasoft Pseudopotentials to the Projector Augmented-Wave Method. *Phys. Rev. B* **1999,** *59*, 1758-1775.
(34) Perdew, J. P.; Burke, K.; Ernzerhof, M., Generalized Gradient Approximation Made Simple. *Phys. Rev. Lett.* **1996,** *77*, 3865.
(35) Henkelman, G.; Arnaldsson, A.; Jónsson, H., A Fast and Robust Algorithm for Bader Decomposition of Charge Density. *Comput. Mater. Sci.* **2006,** *36*, 354-360.
(36) Yu, M.; Trinkle, D. R., Accurate and Efficient Algorithm for Bader Charge Integration. *J. Chem. Phys.* **2011,** *134*, 064111.
(37) Grimme, S.; Antony, J.; Ehrlich, S.; Krieg, H., A Consistent and Accurate Ab Initio Parametrization of Density Functional Dispersion Correction (DFT-D) for the 94 Elements H-Pu. *J. Chem. Phys.* **2010,** *132*, 154104.
(38) Nosé, S., A Unified Formulation of the Constant Temperature Molecular Dynamics Methods. *J. Chem. Phys.* **1984,** *81*, 511-519.
(39) Hoover, W. G., Canonical Dynamics: Equilibrium Phase-Space Distributions. *Phys. Rev. A* **1985,** *31*, 1695-1697.
(40) Li, Y.; Liu, Z.-F., Cross-Sphere Electrode Reaction: The Case of Hydroxyl Desorption during the Oxygen Reduction Reaction on Pt(111) in Alkaline Media. *J. Phys. Chem. Lett.* **2021,** *12*, 6448-6456.
(41) Woo, T. K.; Margl, P. M.; Blöchl, P. E.; Ziegler, T., A Combined Car−Parrinello QM/MM Implementation for *Ab Initio* Molecular Dynamics Simulations of Extended Systems: Application to Transition Metal Catalysis. *J. Phys. Chem. B* **1997,** *101*, 7877-7880.
(42) Jarzynski, C., Nonequilibrium Equality for Free Energy Differences. *Phys. Rev. Lett.* **1997,** *78*, 2690-2693.
(43) Sprik, M.; Ciccotti, G., Free Energy from Constrained Molecular Dynamics. *J. Chem. Phys.* **1998,** *109*, 7737-7744.
(44) Hassanali, A. A.; Cuny, J.; Verdolino, V.; Parrinello, M., Aqueous Solutions: State of the Art in *Ab Initio* Molecular Dynamics. *Philos. Trans. R. Soc. A* **2014,** *372*, 20120482.
(45) Skúlason, E.; Karlberg, G. S.; Rossmeisl, J.; Bligaard, T.; Greeley, J.; Jónsson, H.; Nørskov, J. K., Density Functional Theory Calculations for the Hydrogen Evolution Reaction in an Electrochemical Double Layer on the Pt(111) Electrode. *Phys. Chem. Chem. Phys.* **2007,** *9*, 3241-3250.
(46) Rossmeisl, J.; Skúlason, E.; Björketun, M. E.; Tripkovic, V.; Nørskov, J. K., Modeling the Electrified Solid–Liquid Interface. *Chem. Phys. Lett.* **2008,** *466*, 68-71.
(47) Huang, J. E.; Li, F.; Ozden, A.; Sedighian Rasouli, A.; García de Arquer, F. P.; Liu, S.; Zhang, S.; Luo, M.; Wang, X.; Lum, Y.; Xu, Y.; Bertens, K.; Miao, R. K.; Dinh, C.-T.; Sinton, D.; Sargent, E. H., CO_2 Electrolysis to Multicarbon Products in Strong Acid. *Science* **2021,** *372*, 1074-1078.
(48) Chan, K.; Nørskov, J. K., Electrochemical Barriers Made Simple. *J. Phys. Chem. Lett.* **2015,** *6*, 2663-2668.
(49) Bondue, C. J.; Graf, M.; Goyal, A.; Koper, M. T. M., Suppression of Hydrogen Evolution in Acidic Electrolytes by Electrochemical CO_2 Reduction. *J. Am. Chem. Soc.* **2021,** *143*, 279-285.
(50) Ovalle, V. J.; Hsu, Y.-S.; Agrawal, N.; Janik, M. J.; Waegele, M. M., Correlating Hydration Free Energy and Specific Adsorption of Alkali Metal Cations during CO_2 Electroreduction on Au. *Nat. Catal.* **2022,** *5*, 624-632.

(51) Li, P.; Jiang, Y.; Hu, Y.; Men, Y.; Liu, Y.; Cai, W.; Chen, S., Hydrogen Bond Network Connectivity in the Electric Double Layer Dominates the Kinetic pH Effect in Hydrogen Electrocatalysis on Pt. *Nat. Catal.* **2022**, 1-12.
(52) Monteiro, M. C. O.; Goyal, A.; Moerland, P.; Koper, M. T. M., Understanding Cation Trends for Hydrogen Evolution on Platinum and Gold Electrodes in Alkaline Media. *ACS Catal.* **2021,** *11*, 14328-14335.
(53) Rosen, B. A.; Salehi-Khojin, A.; Thorson, M. R.; Zhu, W.; Whipple, D. T.; Kenis, P. J. A.; Masel, R. I., Ionic Liquid-Mediated Selective Conversion of CO_2 to CO at Low Overpotentials. *Science* **2011,** *334*, 643-644.